Interpolymer Complexation as a Strategy for Nanoparticle Assembly and Crystallization

Srikanth Nayak,[†] Nathan Horst,[‡] Honghu Zhang,[a¶] Wenjie Wang,[¶] Surya Mallapragada,[†] Alex Travesset,[§] and David Vaknin[*,§]

[†]*Ames Laboratory, and Department of Chemical and Biological Engineering, Iowa State University, Ames, Iowa 50011, United States*

[‡]*Ames Laboratory, and Department of Materials Science and Engineering, Iowa State University, Ames, Iowa 50011, United States*

[¶]*Division of Materials Sciences and Engineering, Ames Laboratory, USDOE, Ames, Iowa 50011, United States*

[§]*Ames Laboratory, and Department of Physics and Astronomy, Iowa State University, Ames, Iowa 50011, United States*

E-mail: vaknin@ameslab.gov

[a]Currently at Center for Functional Nanomaterials, Brookhaven National Laboratory, Upton, NY-11973, United States

Abstract

Controlled self-assembly of nanoparticles into ordered structures is a major step in fabricating nanotechnology based devices. Here, we report on the self-assembly of high quality superlattices of nanoparticles in aqueous suspensions induced via interpolymer complexation. Using small angle X-ray scattering, we demonstrate that the NPs crystallize into superlattices of FCC symmetry, initially driven by hydrogen bonding and subsequently by van der Waals forces between the complexed coronas of

hydrogen-bonded polymers. We show that the lattice constant and crystal quality can be tuned by polymer concentration, suspension pH and the length of polymer chains. Interpolymer complexation to assemble nanoparticles is scalable, inexpensive, versatile and general.

Introduction

Assembling nanoparticles into ordered structures is essential for applications in photonics, magnetic storage, spintronics, and other applications.[1–3] Thus, self-assembly of nanoparticles into ordered lattices (superlattices), where large scale ordered structures can be realized, has been the focus of research across multiple disciplines.[2,4] Specifically, self-assembly of metallic nanoparticles and quantum dots have been explored to obtain tunable optical properties.[5,6] A few approaches to achieving ordered structures have been developed including, solvent evaporation,[1] DNA base-pairing,[7] biphasic-separation of water soluble polymers,[8,9] and covalent crosslinking with small molecules.[10] Among these, two of the illustrative approaches for 3D assembly of nanoparticles into superlattices are 1) solvent evaporation induced assembly and 2) DNA-mediated assembly. Both methods have led to the formation of exquisite superlattices by engineering the core sizes, shapes and ligand structure.[11–14] While solvent evaporation based assembly is driven mainly by ligand-entropy and van der Waals forces (vdW),[14,15] DNA-mediated assembly is driven by maximizing Watson-Crick base-pairing.[7]

Various water soluble polymers (charged or neutral) are commonly used as nanoparticle stabilizers and surface modifiers that enable tunable interactions.[16] Recently, we have shown that poly(ethylene glycol) functionalized gold nanoparticles (AuNP-PEG) dispersed in aqueous solutions can be assembled into 2D and 3D superlattices by controlling ionic strength.[8,9] Extending this approach to tune the interactions among the functionalized NPs may be achieved by introducing other polymers that can form inter-polymer complexes (IPCs). Inter-polymer complexes consist of two distinct polymers that interact by non-covalent interactions, such as hydrogen bonds, and have been studied extensively,[17] especially

for pharmaceutical applications.[18]

It has been long recognized that IPCs show recognition properties similar to DNA strands.[19] There is a very large family of polymers that can form IPCs, but whether they can be used for nanoparticle superlattice engineering remains an outstanding question. Despite some efforts to leverage IPCs to assemble nanoparticles,[20,21] as per our knowledge, no examples of long-range structures have been reported. Here, we show that AuNP-PEG in the presence of poly(acrylic acid) (PAA) self-assembles into 3D superlattices (the concept is depicted in Fig. 1). We conduct small angle X-ray scattering (SAXS) and systematically vary the PEG chain length and nanoparticle core size.

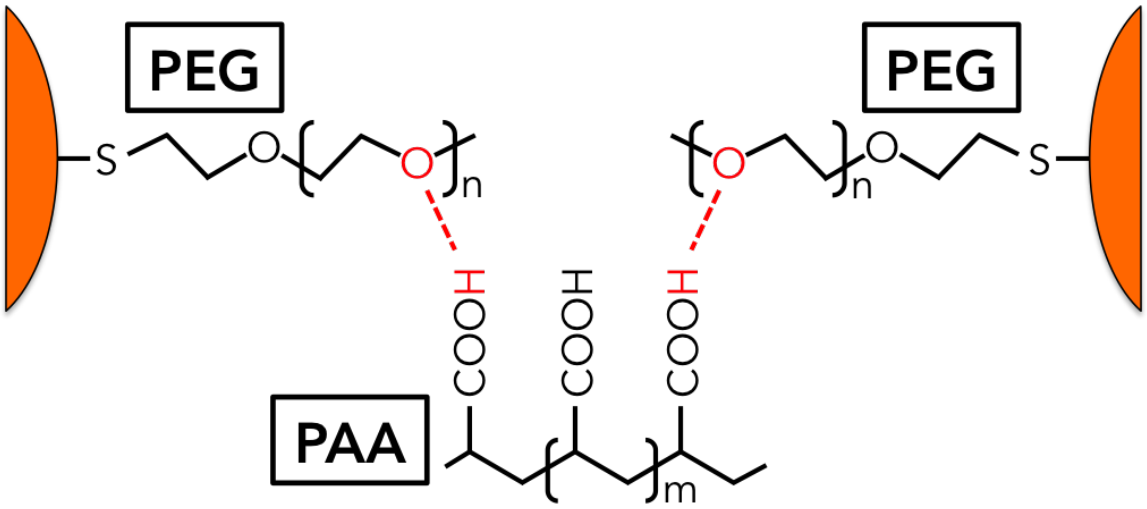

Figure 1: Depiction of inter-polymer complexes between the end tethered PEG chains and free PAA leading to self-assembly of nanoparticles into superlattices.

Experimental Section

Materials: Gold nanoparticles (AuNPs) of 5 and 10 nm nominal diameters, referred to as AuNP5 and AuNP10 respectively, were purchased from Ted Pella Inc. Poly(ethylene glycol) methyl ether thiol (mPEG-SH) with molecular weight (M_n) of $\sim$ 800 Da and $\sim$ 2000 Da (referred to as PEG800 and PEG2000, respectively) and poly(acrylic acid), $M_n \sim 2000$ Da, 50 wt% in water (PAA2000) were purchased from Sigma Aldrich. Poly(ethylene glycol) methyl

ether thiol with M_n of $\sim$ 5000 Da (PEG5000) was purchased from CreativePEGWorks Inc.

Synthesis of assemblies Gold nanoparticles were functionalized with mPEG-SH using the ligand exchange method. Gold nanoparticles were mixed with aqueous solutions of mPEG-SH such that molar ratio of nanoparticles to mPEG-SH is 1:25000 and the mixture was incubated in dark under rotoshaking for $\sim$ 48 hours. Unbound mPEG-SH was separated by dialysis against water for 48 hours using Slide-a-lyzer dialyser cassettes (10000 MWCO). To 0.98 ml of the functionalized nanoparticles, 10 μL of PAA at appropriate concentrations were added and mixed by vortex mixing. After 1 minute of addition of PAA, 10 μL of hydrochloric acid (HCl) at appropriate concentrations were added and mixed again by vortex mixing. The solution was left to stand at room temperature for more than 3 days. The samples are labeled as AuNPx-PEGy, a mM PAA2000, b mM HCl, where x = nominal nanoparticle core diameter in nm, y = M_n of PEG, a = concentration of PAA2000, and b = concentration of HCl. Assemblies aggregate at the bottom of the vial and were collected with a glass pipette and transferred to a quartz capillary, along with the solution from which they are made. The assemblies are in a "wet" state during characterization.

Characterization methods: Small angle X-ray scattering (SAXS) measurements of the precipitates were conducted at beamline 12-ID-B of Advanced Photon Source, Argonne National Laboratory. Samples were contained in 2 mm OD quartz capillaries and the measurements were done at room temperature. Measurements were made in transmission mode with photon energy, $E = 13.3$ keV ($\lambda = 0.9322$ Å) using 2D Pilatus2m detector. Scattering angle was calibrated with silver behenate powder standard. Whereas in-situ imaging of NPs assemblies in suspensions is still a challenge, the SAXS technique is well suited for in-situ structural characterization of the assemblies in their "wet" state.

UV-vis absorbance spectra of the suspensions were measured with Molecular Devices SpectraMax spectrometer, using polystyrene cuvettes. Dynamic light scattering (DLS) measurements were conducted with Malvern Zetasizer Nano-ZS90 (HeNe laser, wavelength = 633 nm, 90^o scattering angle).

Results and Discussions

We find that nanoparticle assemblies are formed by the addition of PAA and HCl to the AuNP-PEG suspensions. At varying concentrations of each constituent, color change and aggregation are visible, followed by precipitation. Samples are collected from this mixture and transferred to quartz capillaries for SAXS measurements (more details are found in the Experimental Section, and the Supporting Information). Nanoparticles are labeled as AuNPx-PEGy, where x refers to the nominal core diameter of the nanoparticle in nanometers, and y refers to the molecular weight of poly(ethylene glycol) used to functionalize the nanoparticles. Assembly conditions are indicated with the concentrations of PAA and HCl in the final solution. More details about sample preparation can be found in the Supporting Information.

SAXS characterization of the assemblies shows the emergence of crystalline structure in the assemblies that can be tuned by the length of the PEG chains. Figure 2(a) shows the structure factor obtained by standard data reduction of SAXS patterns (as the one shown in the inset) for assemblies formed with AuNP10-PEG2000 at 2 mM PAA and 1 mM HCl. Clear diffraction rings in the 2D pattern with distinct peaks in the structure factor emerge, indicating a crystalline structure. To analyze the diffraction pattern, we use a model structure factor[22] as used in an earlier work on crosslinked AuNP assemblies using dithiol chains.[10] The best fit model to the diffraction pattern both in terms of peak positions and intensities is a face-centered-cubic (FCC) lattice with a primary peak at $q_0 \simeq 0.038$ Å^{-1}, and a lattice constant $a \simeq 286$ Å. The nearest neighbor (NN) distance is thus $D_n = \frac{\sqrt{6}\pi}{q_0} \simeq 203$ Å. From the full width at half maximum of the Lorentzian shaped peaks used in the fit, we obtain an average crystallite size using Scherrer equation to be ~ 2900 Å.

Assemblies are also obtained with nanoparticles functionalized with shorter PEG (PEG800)

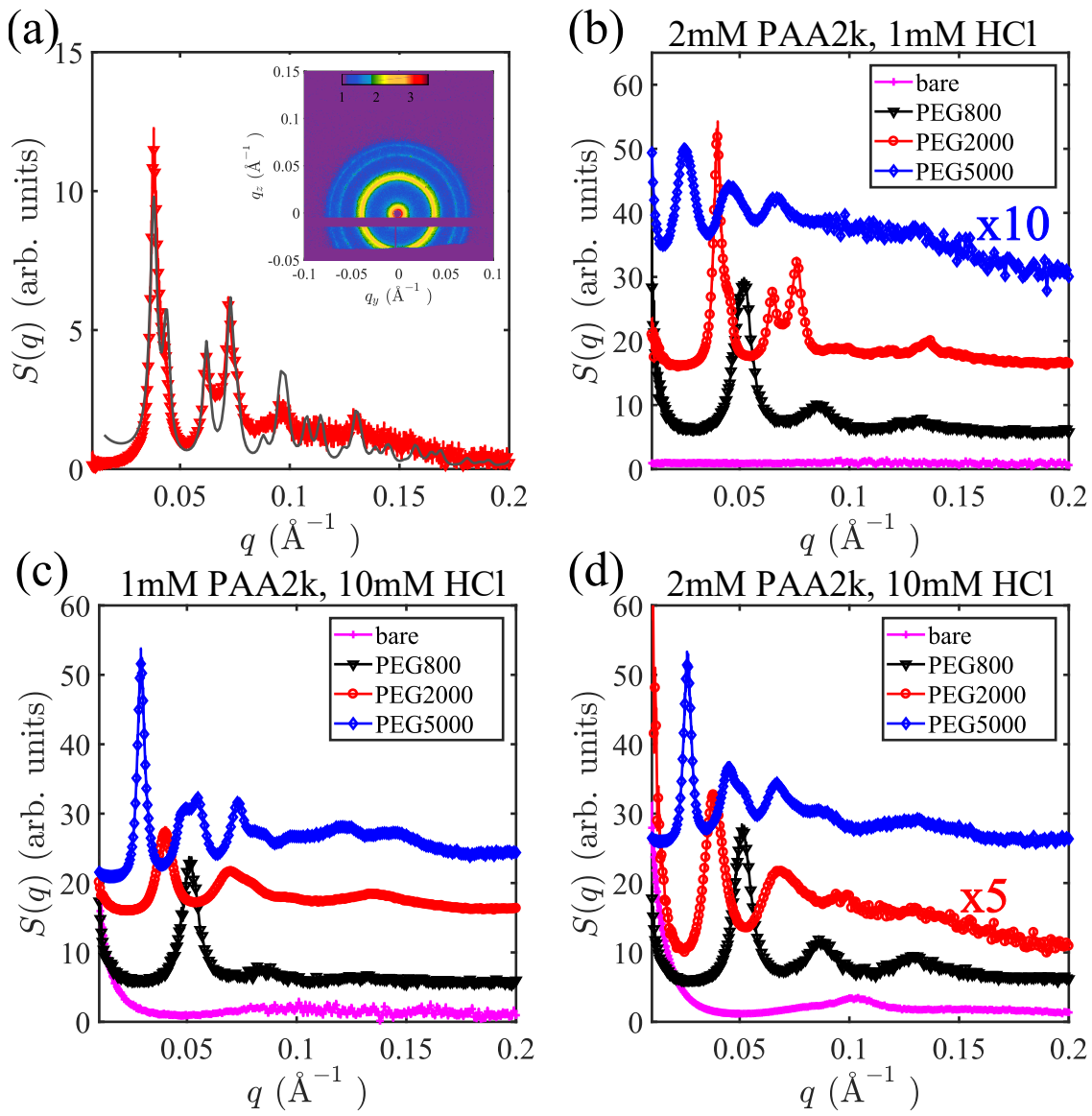

Figure 2: (a) Structure factor curve for AuNP10-PEG2000, 2mM PAA2000, 1mM HCl (red symbols) and the model fit (solid line) for an FCC lattice. (inset) Raw SAXS data shown here with scattering intensity shown on a logarithmic color scale. Structure factor curves obtained from the SAXS data for gold nanoparticles coated with different lengths of PEG-thiol at (b) 2mM PAA2000 and 1mM HCl, (c) 1mM PAA2000 and 10mM HCl, and (d) 2mM PAA2000 and 10mM HCl. Curves are vertically shifted for clarity. Structure factor for AuNP10-PEG2000 in (b) and AuNP10-PEG5000 in (c) are characterized as FCC, while the other diffraction profiles are consistent with FCC structure with stacking faults along the (111) planes.

and longer PEG (PEG5000) for which the position of the primary peak (q_0) decreases with the length of the PEG chains as shown in Figure 2(b-d). Further, the quality of the crystal is found to depend on the concentration of PAA and HCl in the suspension. Table 1 shows characteristic length scales of unit cells under close to optimal crystallization conditions. A full list of conditions explored and the obtained results are presented in Table S2 and Table

S3. All structure factors for PEG-AuNPs assemblies shown in Figure 2 display Bragg-like reflection peaks indicating 3D superlattice formation. By increasing PEG length alone under otherwise identical PAA and HCl concentrations, the resulting superlattice diffraction profiles become more well defined and can be clearly indexed as FCC under favorable conditions (see Fig2.(b) and (c)). In all the cases, the relative peak positions are consistent with FCC structure, although in some cases they are not very well defined indicating poor crystallinity, possibly due to stacking faults. For 10 nm nominal AuNPs the center-to-center inter-particle distance ranges from ~ 15 nm to ~ 27 nm with different PEG chain lengths.

Table 1: Lattice constant $a = \frac{\sqrt{12}\pi}{q_0}$, and nearest neighbor ($D_n = \frac{\sqrt{6}\pi}{q_0}$) with 95% confidence intervals, extracted from SAXS for AuNP-PEG of different PEG lengths obtained in the presence of 1 mM PAA2000 at 10 mM HCl. The hydrodynamic radius D_H obtained from DLS is obtained without PAA and HCl. The values in parentheses represent the distribution of hydrodynamic size of the grafted particles. Actual diameter of the nominal 10 and 5 nm AuNP obtained from SAXS are AuNP diameter $D = 8.8 \pm 0.8$ and 6.3 ± 0.9 nm respectively.

Nanoparticle	a (Å)	D_n (Å)	D_H (Å)
AuNP10	-	-	139(37)
AuNP10-PEG800	214 ± 1	151 ± 1	186(48)
AuNP10-PEG2000	272 ± 2	192 ± 1	249(63)
AuNP10-PEG5000	376 ± 1	266 ± 1	408(121)
AuNP5-PEG2000	225 ± 1	159 ± 1	205(35)

To gain insight into the assembly mechanism, we determine the variation of NN distances in the assembly as a function of PEG chain length experimentally and compare the results with expected trends for vdW and hydrogen bonding dominated assemblies. For structures with local coordination larger than 6, such as FCC, the orbifold topological model (OTM)[23] predicts that the dimensionless NN distance, τ_{OPM} (D_n/D; D is the nanoparticle core diameter) is given by optimal packing model (OPM)[24]

$$\tau_{OPM} = (3\xi\lambda + 1)^{\frac{1}{3}}, \tag{1}$$

where, $\xi = \frac{A_0}{A} \approx 1$ (A_0 is the cross section of the polymer ≈ 20 Å^2 and A is actual area occupied by a bound polymer to the NP surface; $1/\xi$ = dimensionless grafting density) and $\lambda = 2L/D$ (L is the polymer contour length and D is the NP diameter). The 1/3 exponent reflects the optimization of the packing fraction that follows from vdW attractive forces. In

contrast, in DNA-mediated assembly where the structure is stabilized by hydrogen bonds, the NN distances are found to be linearly dependent on the DNA length.[25,26]

Figure 3 shows SAXS extracted dimensionless NN-distances *versus* dimensionless PEG contour-length and the theoretical OTM/OPM curve (Eq. (1)) with no fitting parameters. The $\tau = 1+\lambda$ line refers to the NN-distance assuming the PEG chains are fully stretched and there is no overlap of PEG coronas, and hence is the maximum distance between NPs. The close match between the experimentally observed and the predictions from the OTM/OPM suggests that the formation of PAA-PEG IPCs hampers the ability of water molecules to form hydrogen bonds with either polymer, leading to a relatively dry superlattice that is stabilized by vdW forces, just as it is the case for polystyrene and hydrocarbon capped nanocrystals obtained from solvent evaporation.[14,23] In Fig. 3, data from assemblies obtained by solvent evaporation in polystyrene functionalized gold nanoparticles[14] also follow the OTM/OPM curve.[23] This, combined with the need for low pH for the formation of assemblies, indicate that the assembly is initially driven by hydrogen bonds, and as the aggregates become solvent free, vdW forces establish a close to optimal packing FCC structure. Our results contrast with those of DNA mediated assemblies, where NN distance is much larger than that predicted by OPM (blue line in Fig. 3, obtained from Hill et al.[25]) as it is known that the superlattice is swollen with more than 90% interstitial water.[12]

Our results show that the formation of ordered assemblies depends on all the tested parameters, namely, molecular weight of PEG, concentration of PAA and HCl. The critical pH, at which IPCs formed by linear chains of PAA and PEG phase separate, depends on the molecular weight and concentration of the polymers.[27]NP assembly is achieved for charge-neutral PAA implying the formation of hydrogen bonds in the initial assembly process. In addition, OPM results suggest that the vdW forces play a role in the stability of assemblies of PAA-PEG-AuNPs complexes. This is consistent with fluorescence and UV spectroscopy studies of IPCs of free, non-grafted PAA-PEG polymers.[28,29] Although there are qualitative similarities in the formation of IPCs in both scenarios (i.e., with linear PAA and PEG in bulk,

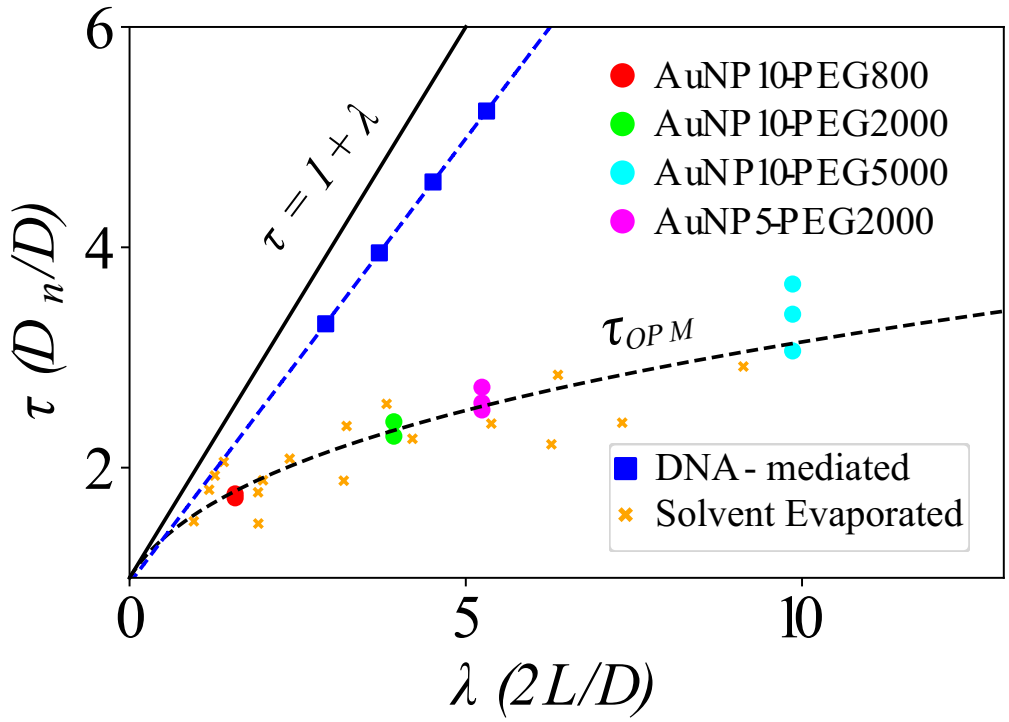

Figure 3: Dimensionless nearest neighbor distances ($\tau = \frac{D_n}{D} = \frac{\sqrt{6}\pi}{q_0 D}$; q_0 is the primary peak position in SAXS and D is the nanoparticle diameter) plotted against dimensionless contour length of PEG ($\lambda = \frac{2L}{D}$; L is the contour length of the PEG chain). We plot the result of the OTM/OPM model (Eq. 1) to show that our data agrees without the use of any fitting parameters. Solid black line refers to the maximum possible distance between the nanoparticles. Red, green, magenta and turquoise circles are the experimentally obtained points for AuNP10-PEG800, AuNP10-PEG2000, AuNP10-PEG5000, and AuNP5-PEG2000 respectively. The black dashed line is the prediction from OTM/OPM. The blue dashed line is the variation of NN distance with the DNA linker length in DNA-mediated assemblies, obtained by using equation (2) provided in reference.[25] The orange xs refer to the data points obtained from reference[14] for the solvent evaporation system with poly(styrene) functionalized AuNPs. The figure implies that the formation of PAA-PEG hydrogen bonds leads to a dehydration of the superlattice and its subsequent stabilization by vdW forces.

versus grafted PEG on NPs with PAA) there are some notable differences. For PAA/PEG IPCs in bulk, at a fixed monomer concentration and PAA length, there is a minimum molecular weight of $\sim$ 6000Da of PEG required to form IPCs.[17,30] This dependence on molecular weight has been attributed to the higher loss of translational entropy for the shorter polymers and the co-operative behavior of hydrogen bond formation in the complexes.[31,32] In contrast, we find that assemblies are formed even with 800 Da AuNP-PEG. Although not forming superlattices, even shorter (3 or 6-mer) AuNP-oligoEG show pH-responsive assembly in the presence of PAA.[21] Further, an excess of PAA (in base-moles) is required for the formation of NP assembly (Table.S4), as opposed to the equimolar proportions required in the formation of IPCs of PAA /PEG in bulk solution.[18]

Conclusion

In this work, we have demonstrated the formation of FCC crystals of AuNPs functionalized with PEG via interpolymer complexes with PAA. The NN distances in the superlattices primarily depend on the length/molecular-weight of PEG and hence are tunable. Further, the conditions (pH and PAA concentration) for the formation of the assemblies depend on the PEG molecular weight. Theoretical considerations of the dependence of NN distance on the PEG chain length suggest that van der Waals forces that arise due to the formation of IPCs play a significant role in the stability of the assemblies. IPCs have been shown to form with several polymers such as poly(N-isopropylacrylamide), poly(N-vinylpyrrolidone), and polysaccharides.[18] Since these polymers are commonly used in NP functionalization and stabilization, our results open a potential route for the assembly of a wide variety of NPs. These results also raise several possibilities such as obtaining binary superlattices using different cores and ligands, and using block copolymers instead of PAA homopolymers. Thus, this work brings new tools for controlling and directing the self-assembly of nanoparticles.

Acknowledgement

We thank Dr. Xiaobing Zuo for technical support with the SAXS measurements. Research was supported by the U.S. Department of Energy (U.S. DOE), Office of Basic Energy Sciences, Division of Materials Sciences and Engineering. Ames Laboratory is operated for the U.S. DOE by Iowa State University under Contract No. DE-AC02-07CH11358. Use of the Advanced Photon Source, an Office of Science User Facility operated for the U.S. DOE Office of Science by Argonne National Laboratory, was supported by the U.S. DOE under Contract No. DE-AC02-06CH11357.

Supporting Information

Supporting Information Available: Supporting Information provides the following: 1) Complementary experiments explaining in more detail sample preparation and characterization including DLS, UV-vis, and SAXS data reduction, 2) Results on the explored conditions, and 3) Detail on the OTM model. This material is available free of charge via the Internet at `http://pubs.acs.org`.

References

(1) Talapin, D. V.; Lee, J. S.; Kovalenko, M. V.; Shevchenko, E. V. Prospects of colloidal nanocrystals for electronic and optoelectronic applications. *Chemical Reviews* **2010**, *110*, 389-458.

(2) Boles, M. A.; Engel, M.; Talapin, D. V. Self-assembly of colloidal nanocrystals: From intricate structures to functional materials. *Chemical Reviews* **2016**, *116*, 11220-11289.

(3) Sun, L.; Lin, H.; Kohlstedt, K. L.; Schatz, G. C.; Mirkin, C. A. Design Principles for

photonic crystals based on plasmonic nanoparticle superlattices. *Proc. Natl. Acad. Sci. U. S. A.* **2018**, *115*, 7242.

(4) Nie, Z. H.; Petukhova, A.; Kumacheva, E. Properties and emerging applications of self-assembled structures made from inorganic nanoparticles. *Nat. Nanotechnol.* **2010**, *5*, 15-25.

(5) Ross, M. B.; Ku, J. C.; Lee, B.; Mirkin, C. A.; Schatz, G. C. Plasmonic metallurgy enabled by DNA. *Adv. Mater.* **2016**, *28*, 2790.

(6) Sun, L.; Lin, H.; Park, D. J.; Bourgeois, M. R.; Ross, M. B.; Ku, J. C.; Schatz, G. C.; Mirkin, C. A. Polarization-dependent optical response in anisotropic nanoparticle DNA superlattices. *Nano Letters* **2017**, *17*, 2313-2318.

(7) Macfarlane, R. J.; Lee, B.; Jones, M. R.; Harris, N.; Schatz, G. C.; Mirkin, C. A. Nanoparticle superlattice engineering with DNA. *Science* **2011**, *334*, 204-208.

(8) Zhang, H.; Wang, W.; Mallapragada, S.; Travesset, A.; Vaknin, D. Macroscopic and tunable nanoparticle superlattices. *Nanoscale* **2016**, *9*, 164-171.

(9) Zhang, H.; Wang, W.; Akinc, M.; Mallapragada, S.; Travesset, A.; Vaknin, D. Assembling and ordering polymer-grafted nanoparticles in three dimensions. *Nanoscale* **2017**, *9* , 8710-8715.

(10) Nayak, S.; Horst, N.; Zhang, H.; Wang, W.; Mallapragada, S.; Travesset, A.; Vaknin, D. Ordered networks of gold nanoparticles crosslinked by dithiol-oligomers. *Part. Part. Syst. Charact.* **2018**, 1800097.

(11) Park, S. Y.; Lytton-Jean, A. K. R.; Lee, B.; Weigand, S.; Schatz, G. C.; Mirkin, C. A. DNA-programmable nanoparticle crystallization. *Nature* **2008**, *451*, 553.

(12) Nykypanchuk, D.; Maye, M. M.; van der Lelie, D.; Gang, O. DNA-guided crystallization of colloidal nanoparticles. *Nature* **2008**, *451*, 549-552.

(13) Tian, Y.; Zhang, Y.; Wang, T.; Xin, H.; Li, H. L.; Gang, O. Lattice engineering through nanoparticle-DNA frameworks. *Nat. Mater.* **2016**, *15*, 654.

(14) Ye, X. C.; Zhu, C. H.; Ercius, P.; Raja, S. N.; He, B.; Jones, M. R.; Hauwiller, M. R.; Liu, Y.; Xu, T.; Alivisatos, A. P. Structural diversity in binary superlattices self-assembled from polymer-grafted nanocrystals. *Nat. Commun.* **2015**, 6.

(15) Bodnarchuk, M. I.; Kovalenko, M. V.; Heiss, W.; Talapin, D. V. Energetic and entropic contributions to self-assembly of binary nanocrystal superlattices: temperature as the structure-directing factor. *J. Am. Chem. Soc.* **2010**, *132*, 11967-11977.

(16) Si Kae, J.; Chen, Y.; Shi, Q.; Cheng, W. Nanoparticle superlattices: the roles of soft ligands. *Adv. Sci.* **2018**, *5*, 1700179.

(17) Kabanov, V. A.; Papisov, I. M. Formation of complexes between the complementary synthetic polymers and oligomers in dilute solutions. *Vysokomolekulyarnye Soedineniya Seriya A* **1979**, *21*, 243-281.

(18) Hydrogen-bonded interpolymer complexes : Formation, structure and applications; Vitaliy V. Khutoryanskiy, Georgios Staikos Eds.; World Scientific: Singapore, **2009**.

(19) Litmanovich, A. A.; Papisov, I. M.; Kabanov, V. A. "Recognition" of copolymers and stereoisomers in macromolecule complexation reactions in dilute solutions. *Eur. Polym. J.* **1981**, *17*, 981-988.

(20) Irmukhametova, G. S.; Fraser, B. J.; Keddie, J. L.; Mun, G. A.; Khutoryanskiy, V. V. Hydrogen-bonding driven self-assembly of PEGylated organosilica nanoparticles with poly(acrylic acid) in aqueous solutions and in layer-by-layer deposition at solid surfaces. *Langmuir* **2012**, *28*, 299-306.

(21) Torii, Y.; Sugimura, N.; Mitomo, H.; Niikura, K.; Ijiro, K. pH-responsive coassembly

of oligo(ethylene glycol)-coated gold nanoparticles with external anionic polymers via hydrogen bonding. *Langmuir* **2017**, *33*, 5537.

(22) Senesi, A. J.; Lee, B. Small-angle scattering of particle assemblies. *J. Appl. Crystallogr.* **2015**, *48*, 1172-1182.

(23) Travesset, A.; Topological structure prediction in binary nanoparticle superlattices *Soft Matter* **2017**, *13* 147-157.

(24) Landmann, U; Luedtke, W. D. Small is different: Energetic, structural, thermal, and mechanical properties of passivated nanocluster assemblies *Faraday Discuss.* **2004** *125* 1-22.

(25) Hill, H. D.; Macfarlane, R. J.; Senesi, A. J.; Lee, B.; Park, S. Y.; Mirkin, C. A. Controlling the lattice parameters of gold nanoparticle FCC crystals with duplex DNA linkers. *Nano Letters* **2008**, *8* , 2341-2344.

(26) Knorowski, C.; Burleigh, S.; Travesset, A. Dynamics and statics of DNA-programmable nanoparticle self-assembly and crystallization *Phys. Rev. Lett.* **2011**, *106*.

(27) Khutoryanskiy, V.; Mun, G.; Nurkeeva, Z.; Dubolazov, A. pH and salt effects on interpolymer complexation via hydrogen bonding in aqueous solutions. *Polym. Int.* **2004**, *53*, 1382-1387.

(28) Koussathana, M.; Lianos, P.; Staikos, G. Investigation of hydrophobic interactions in dilute aqueous solutions of hydrogen-bonding interpolymer complexes by steady-state and time-resolved fluorescence measurements. *Macromolecules* **1997**, *30*, 7798-7802.

(29) Khutoryanskiy, V.; Nurkeeva, Z.; Mun, G.; Dubolazov, A. Effect of temperature on aggregation/dissociation behavior of interpolymer complexes stabilized by hydrogen bonds. *J. Appl. Polym. Sci.* **2004**, *93*, 1946-1950.

(30) Antipina, A. D.; Baranovskii, V. Y.; Papisov, I. M.; Kabanov, V. A. Equilibrium peculiarities in the complexing of polymeric acids with poly (ethylene glycols). *Polym. Sci. U.S.S.R.* **1972**, *14*, 1047-1057.

(31) Pradip; Maltesh, C.; Somasundaran, P.; Kulkarni, R.; Gundiah, S. Polymer-polymer complexation in dilute aqueous solutions - poly(acrylic acid)-poly(ethylene oxide) and poly(acrylic acid)-poly(vinyl pyrolidone). *Langmuir* **1991**, *7*, 2108-2111;.

(32) Hao, J.; Yuan, G.; He, W.; Cheng, H.; Han, C.; Wu, C. Interchain hydrogen-bonding-induced association of poly(acrylic acid)-graft-poly(ethylene oxide) in water. *Macromolecules* **2010**, *43*, 2002-2008.

Graphical TOC Entry

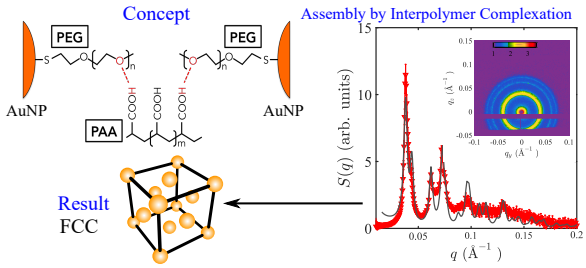

Supporting information

Interpolymer Complexation as a Strategy for Nanoparticle Assembly and Crystallization

Srikanth Nayak[†], Nathan Horst[‡], Honghu Zhang[§1], Wenjie Wang[§], Surya Mallapragada[†], Alex Travesset[||], David Vaknin[||,*]

†*Ames Laboratory, and Department of Chemical and Biological Engineering, Iowa State University, Ames, Iowa 50011, United States*

‡*Ames Laboratory, and Department of Materials Science and Engineering, Iowa State University, Ames, Iowa 50011, United States*

§*Division of Materials Sciences and Engineering, Ames Laboratory, USDOE, Ames, Iowa 50011, United States*

||*Ames Laboratory, and Department of Physics and Astronomy, Iowa State University, Ames, Iowa 50011, United States*

[1]Current address: Center for Functional Nanomaterials, Brookhaven National Laboratory, Upton, NY-11973, United States

1. Complementary experiments

We estimate the core size of the AuNPs from SAXS of the suspension. The form factor of the nanoparticles was obtained by fitting SAXS results from nanoparticle suspension to theoretical scattering from a population of spheres with Gaussian size distribution (Figure S1(a))and it resulted in $R_0 \sim \mathcal{N}(42\ \text{Å}, 4.0^2\ \text{Å}^2)$. We functionalized the gold nanoparticles with thiol terminated PEG using ligand exchange method and obtained the nanoparticle concentration and the hydrodynamic size using UV-vis spectroscopy (extinction at 520 nm) and dynamic light scattering respectively. The results are listed in Table.S1. The hydrodynamic size of the AuNPs increased with increasing PEG chain length upon functionalization as shown in Figure S1(b)).

Table S1: Concentrations of nanoparticles from absorbance value at 520 nm and the hydrodynamic size for gold nanoparticles grafted with different mPEG-SH chains.

Nanoparticle	Concentration, nM	D_H, nm	PEG chain length, nm
AuNP10	9.3	13.9 ± 3.7	-
AuNP10-PEG800	6.2	18.6 ± 4.8	6.6
AuNP10-PEG2000	6.2	24.9 ± 6.3	16.5
AuNP10-PEG5000	5.8	40.8 ± 12.1	41.4
AuNP5-PEG2000	66	20.5 ± 3.5	16.5

PEG brush height on the gold nanoparticles are found by subtracting the gold nanoparticle core size from the hydrodynamic size of the functionalized nanoparticles. Figure S2(a) shows the variation of brush height with number of monomers in PEG. The trend can be approximated by a scaling law with a scaling exponent of ~ 0.6, which indicates that the brushes are in semi-dilute polymer brush regime.[1]

2. SAXS data reduction and summary of results

SAXS data are reduced according to techniques as shown in Figure S3. In the absence of PAA, addition of HCl causes precipitation of non-functionalized AuNPs, but does not affect the PEG functionalized AuNPs, indicating good colloidal stability upon PEG functional-

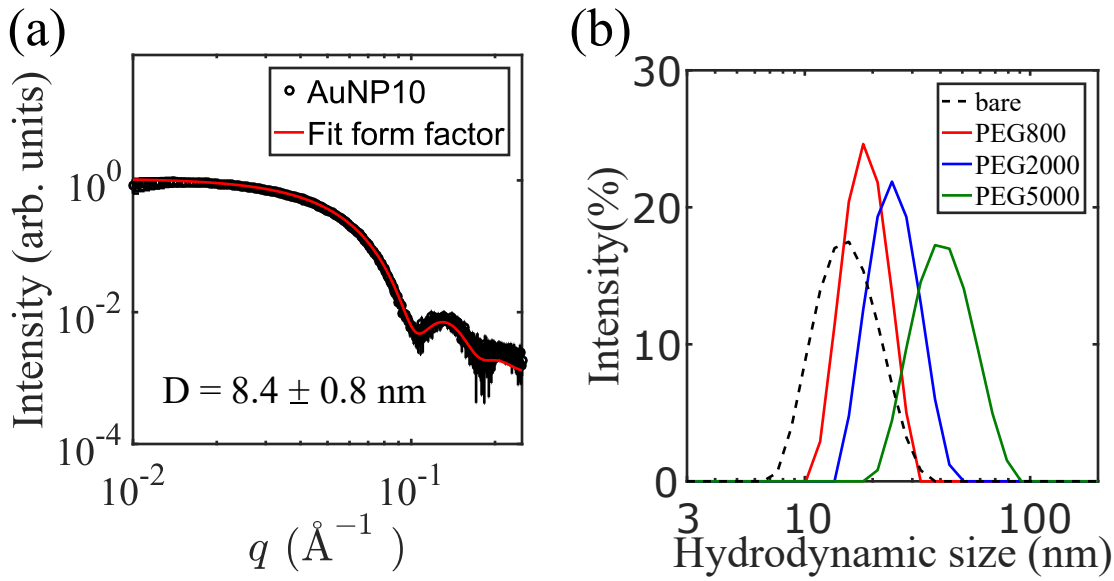

Figure S1: (a) SAXS results for bare AuNPs with nominal diameter of 10 nm after standard data reduction (shown in black circles with error bars) and the form factor fit (solid red line) showing a normal distribution with mean particle diameter, D = 8.4nm and standard deviation = 0.8 nm. For AuNPs with 5 nm nominal diameter the form factor fit results in mean diameter, D = 6.3nm and standard deviation of 0.9 nm.(b) Dynamic light scattering results for bare gold nanoparticles with nominal diameter of 10 nm and the same gold nanoparticles after being functionalized with PEG-thiol of Mn ∼800 Da, ∼2000 Da and ∼5000 Da.

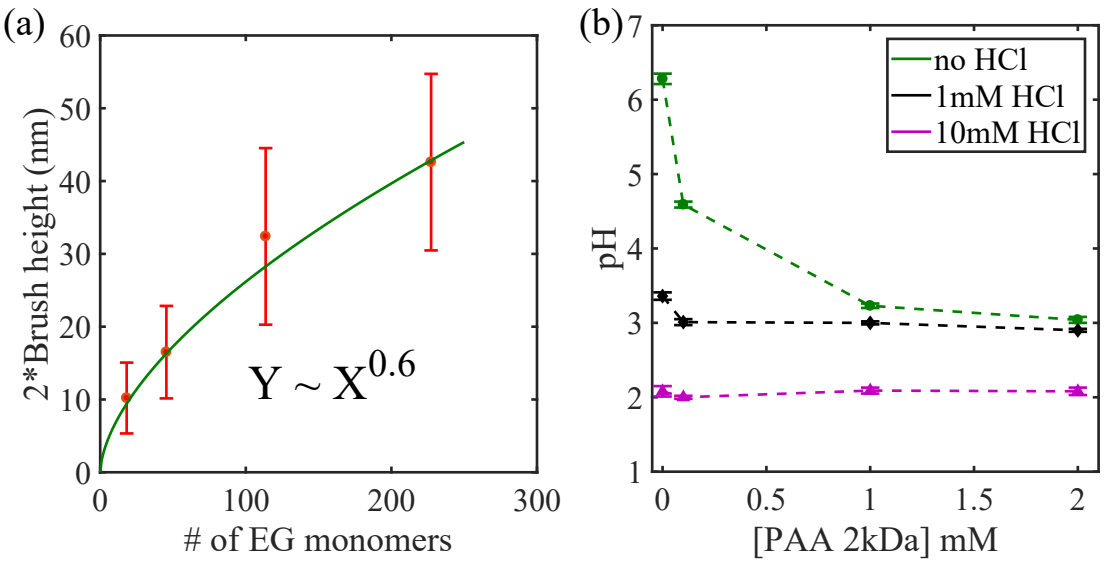

Figure S2: (a) Brush height of PEG chains on gold nanoparticles obtained from hydrodynamic sizes plotted against number of EG monomers in the chain (red circles with error bars). The trend (green line)shows a scaling law behavior with a scaling exponent of ∼ 0.6 indicating that the brushes are in semi-dilute polymer brush (SDPB) regime. PEG10000 shown in these results were not used for the experiment. (b) pH change with increasing concentration of PAA2000 and hydrochloric acid in solution. The dashed lines are to guide the eye. It can be seen from the above plot that at high concentration of HCl, PAA does not affect the pH. Thus, in the presence of HCl, increasing the PAA concentration does not affect the degree of protonation of PAA. Measurements of pH were made in aqueous solutions without nanoparticles.

ization. (Table S2 and Figure S4) Further, the PEG functionalized AuNPs showed varying assembly behavior at different PAA and HCl concentrations.

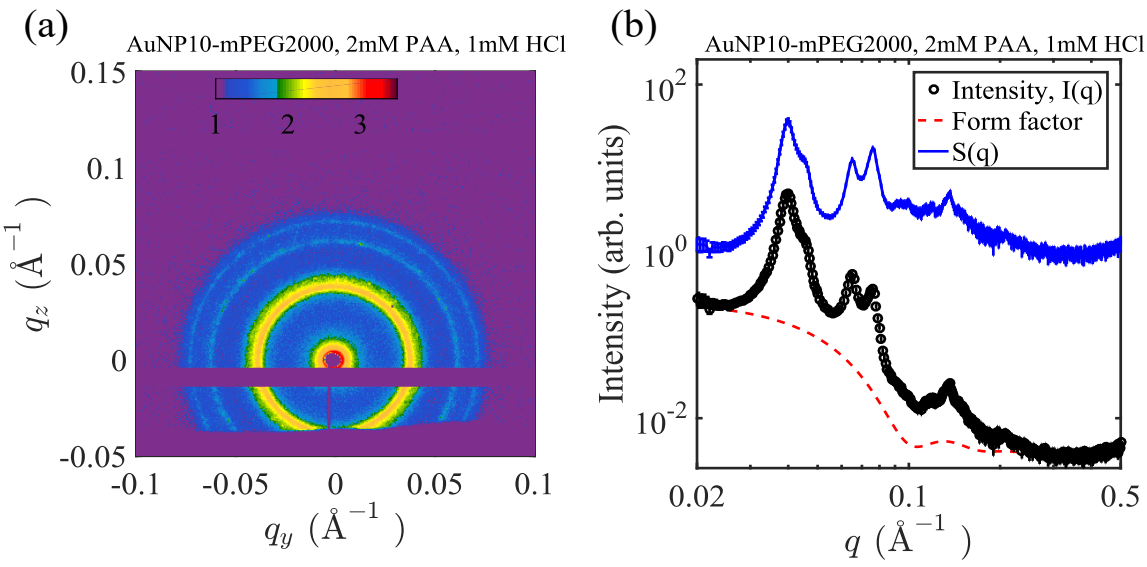

Figure S3: (a) Raw SAXS intensity shown on a logarithmic scale. Standard data reduction techniques to obtain 1D SAXS results were applied on this 2D data. Rings can be clearly seen showing the crystalline nature of the sample. (b) Structure factor S(q) is obtained by removing the form factor from background subtracted intensity data for a sample. Here the procedure is illustrated for sample with AuNP10-PEG2000, 2mM PAA2000 and 1mM HCl.

Table S2: Summary of results for different experimental conditions. Values in the table are the positions of the primary peak in the structure factor curves given in Å^{-1} units. Letters 'A' indicates that the aggregates showed an amorphous structure while 'S' indicates that the nanoparticles did not aggregate and a stable suspension was observed.

Nanoparticle	[PAA2000] (mM)	0 M	1 mM	10 mM
AuNP10	0	S	S	A
AuNP10	0.1	S	S	A
AuNP10	1	S	S	A
AuNP10	2	S	S	A
AuNP10-PEG800	0	S	S	S
AuNP10-PEG800	0.1	S	S	0.051
AuNP10-PEG800	1	0.051	0.051	0.051
AuNP10-PEG800	2	0.051	0.051	0.051
AuNP10-PEG2000	0	S	S	S
AuNP10-PEG2000	0.1	S	S	S
AuNP10-PEG2000	1	S	S	0.04
AuNP10-PEG2000	2	S	0.038	0.038
AuNP10-PEG5000	0	S	S	S
AuNP10-PEG5000	0.1	S	S	S
AuNP10-mEG5000	1	S	S	0.029
AuNP10-PEG5000	2	S	0.027	0.026
AuNP5	1	–	–	A
AuNP5	2	–	–	A
AuNP5-PEG2000	1	S	S	0.048
AuNP5-PEG2000	2	S	0.045	0.047

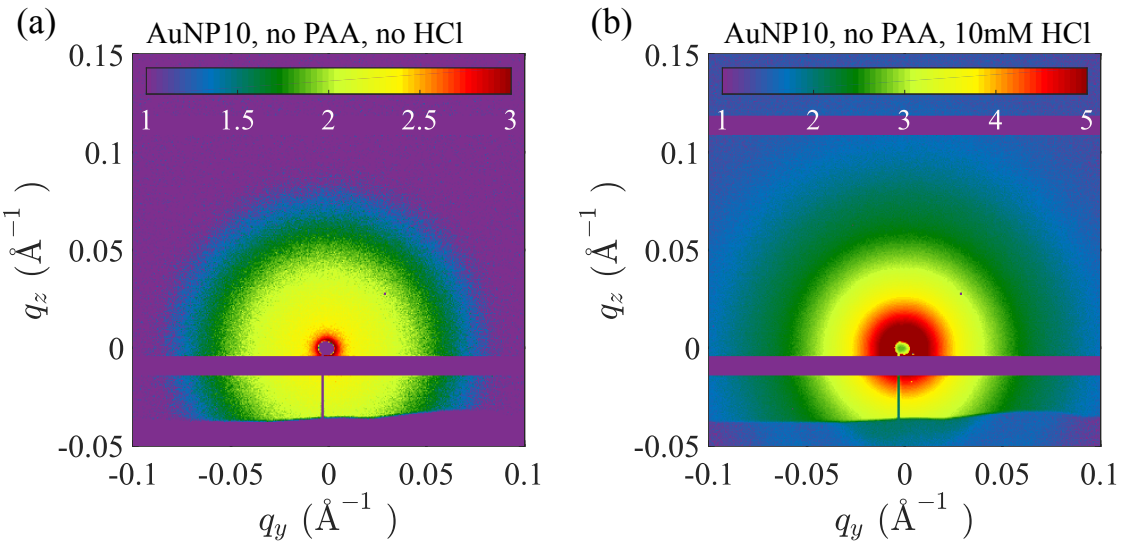

Figure S4: Raw SAXS intensity shown on a logarithmic scale for (a) gold nanoparticles dispersed in suspension (indicated as S in Table S2) and (b) amorphous aggregates (indicated as A in Table S2)

Since the molecular area of a thiol bond on gold is $\simeq 0.25$ nm^2,[2] we estimate that the maximum number of PEG chains on 10 nm AuNPs to be $\sim$ 900/nanoparticle and that for 5 nm AuNPs to be $\sim$ 500/nanoparticle. Concentration of acrylic acid monomers in PAA2000 solutions is ~ 27.7 times the concentration of PAA2000 polymer. Table.S4 shows the estimated ethylene glycol (EG) concentration in the nanoparticle suspensions. Given that 0.1 mM of PAA2000 (2.7mM of AA) was not sufficient in most cases for the assemblies to form, an excess of AA per EG appears necessary.

3. Structure factor model

In this model, A_0 is a constant, free parameter; $\beta(q)$ corrects for particle size polydispersity and orientational disorders;[22] $G(q_{hkl})$ is the Debye Waller factor that allows for translational disorders in the lattice;[22] $Z_0(q_{hkl})$ is the structure factor for an ideal crystal; $L(q : q_{hkl}$ is the shape function (we use Lorentzian shape function) arising due to the finite size of the crystals; and D_n is the nearest neighbor distance. For model simplicity we have assumed the polydispersity of nanoparticle size to have no effect on the structure factor (β(q) = 1).

Table S3: Summary of structure factors obtained for AuNP-PEG systems when a diffraction pattern is observed. PEG length refers to the contour length of the PEG-thiols. D_n is the nearest neighbor distance in the FCC crystal obtained from the position of the primary peak in the structure factor curve. Crystallite size is obtained from the Scherrer equation.

Nanoparticle	PAA2000 (mM)	HCl	PEG length (nm)	$D_n(nm)$	Crystallite size (nm)
AuNP10-PEG800	0.1	10	6.6	15.0	171
AuNP10-PEG800	1	0	6.6	15.1	177
AuNP10-PEG800	1	1	6.6	15.1	172
AuNP10-PEG800	1	10	6.6	15.1	172
AuNP10-PEG800	2	0	6.6	15.1	168
AuNP10-PEG800	2	1	6.6	15.1	164
AuNP10-PEG800	2	10	6.6	15.1	175
AuNP10-PEG2000	1	10	16.5	19.2	191
AuNP10-PEG2000	2	1	16.5	20.3	289
AuNP10-PEG2000	2	10	16.5	20.3	148
AuNP10-PEG5000	1	10	41.4	26.6	300
AuNP10-PEG5000	2	1	41.4	29	159
AuNP10-PEG5000	2	10	41.4	29.6	289
AuNP5-PEG2000	1	10	16.5	15.9	159
AuNP5-PEG2000	2	1	16.5	17.2	-
AuNP5-PEG2000	2	10	16.5	16.4	159

Table S4: Concentration of ethylene glycol (EG) in the nanoparticle assemblies estimated at highest grafting density.

Nanoparticle	[EG] estimated (mM)
AuNP10-PEG800	0.1
AuNP10-PEG2000	0.25
AuNP10-PEG5000	0.6
AuNP5-PEG2000	1.5

Crystallite sizes (C_{FCC}) were calculated using the Scherrer equation (Eq.S2).

$$S_{Mod}(q) = A_0 \sum_{hkl} S(q : q_{hkl}) \tag{S1a}$$

$$S(q : q_{hkl}) = 1 + G(q_{hkl}) \left[\beta(q) Z_0(q_{hkl}) L(q : q_{hkl}, \sigma) - 1\right] \tag{S1b}$$

$$\beta(q) = 1(Assumption) \tag{S1c}$$

$$Z_0(q_{hkl}) = \frac{m_{hkl}}{q_{hkl}^2} \tag{S1d}$$

$$G(q) = \exp\left(-\sigma_D^2 D_n^2 q_{hkl}^2\right) \tag{S1e}$$

$$L(q : q_{hkl}, \sigma) = \frac{\sigma}{2\pi} \frac{1}{(q - q_{hkl})^2 + (\frac{\sigma}{2})^2} \tag{S1f}$$

And the particle size or correlation length is given by the Scherrer formula using the constant $K \approx 0.9$

$$C_{FCC} = \frac{4\pi K}{\sigma} \tag{S2}$$

4. OTM model as applied to IPC mediated assembly

We see that in all cases, the maximum grafting density ($\xi = 1$) is the a better predictor than smaller values of ξ, which prompts us to realize the different possibilities for inter-particle linkage (IPL) as shown in Fig. S5.

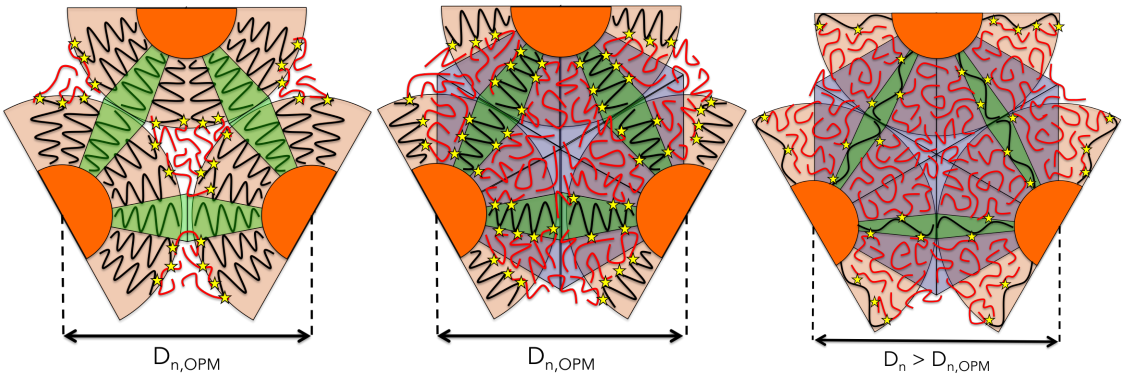

(a) maximum packing density (b) PEG-compressed (c) PEG-stretched

Figure S5: Possible mechanisms of inter-particle linkage (IPL) mediated by direct PAA bridging. The case of maximum grafting density (a) shows PAA chains forming bridges between nanoparticles, but at lower grafting densities, PAA fills unoccupied space, leading to a range of possible D_n values (b,c).

We speculate possible structure of the IPCs in the assemblies as shown in Figure.S5. Figure.S5(a) shows the formation of IPCs when the PEG chains are in the concentrated brush regime (maximum packing density of PEG chains on the AuNPs) where the PAA chains cannot permeate into the corona and the IPCs are at the edges of the PEG corona. When the PEG chains are less densely packed on the AuNPs, PAA chains can permeate and form IPCs within the corona (Fig.S5(b) and (c). Since the tethered PEG chains are in SDPB regime, PAA chains can permeate the PEG corona of the nanoparticles and the PEG chains in the IPCs can be either compressed (Fig.S5(b))or extended (Fig.S5(c)).

References

(1) Dukes, D.; Li, Y.; Lewis, S.; Benicewicz, B.; Schadler, L.; Kumar, S. K. Conformational transitions of spherical polymer brushes: synthesis, characterization, and theory. *Macromolecules* **2010**, *43*, 1564-1570.

(2) Love, J. C.; Estroff, L. A.; Kriebel, J. K.; Nuzzo, R. G.; Whitesides, G. M. Self-assembled monolayers of thiolates on metals as a form of nanotechnology. *Chemical Reviews* **2005**, *105*, 1103-1170.

Graphical TOC Entry